COMMUNICATION

# Push-Pull [7]Helicene Diimide: Excited-State Charge Transfer and Solvatochromic Circularly Polarised Luminescence

Received 00th January 20xx,
Accepted 00th January 20xx

DOI: 10.1039/x0xx00000x

Fridolin Saal,[a] Asim Swain,[a] Alexander Schmiedel,[a] Marco Holzapfel,[a] Christoph Lambert,[a] and Prince Ravat*[,a]

**In this communication we describe a helically chiral push-pull molecule named 9,10-dimethoxy-[7]helicene diimide, displaying fluorescence (FL) and circularly polarised luminescence (CPL) over nearly the entire visible spectrum dependent on solvent polarity. The synthesised molecule exhibits an unusual solvent polarity dependence of FL quantum yield and nonradiative rate constant, as well as remarkable $g_{abs}$ and $g_{lum}$ values along with high configurational stability.**

In the pursuit of chiral functional molecules featuring favourable electronic and optical characteristics, coupled with robust thermal and chemical stability, incorporating imide functionalities onto an aromatic scaffold has emerged as a successful strategy.[1-8] Notable attention has been directed towards exploring the functional properties of chiral imide-containing helicenes.[9-16] Recently we reported a new family of helically chiral diimides, namely, [*n*]helicene diimides ([*n*]HDIs, *n* = 5, 6, and 7).[17] In contrast to their pristine [*n*]helicene analogues,[18, 19] [*n*]HDIs exhibit a remarkable improvement in chiroptical and electrochemical properties. In particular [7]HDI (**1**, Fig. 1) exhibits effective through-bond and through-space conjugation between its terminal imide moieties. This achievement holds significance as it unveils a strategic avenue for mitigating the reduced through-bond conjugation inherent to the twisted structure of helicenes by harnessing the potential of through-space interactions.

Building upon our previous work on [*n*]HDIs, we aim to further amplify the chiroptical properties of these compounds by venturing into the creation of push-pull [*n*]HDIs.[20-22] This strategic endeavour is anticipated to expand our understanding of chiral imide-based molecules and to open new horizons for enhancing their performance and applicability.[23] Herein, we present the synthesis and characterization of a push-pull 9,10-dimethoxy-[7]helicene diimide **2** (Fig. 1). In comparison to **1**, where the methoxy groups are located on the inner helix, compound **2** possesses methoxy groups at the outer rim of the central benzene ring and exhibits distinct photophysical and electrochemical properties. The push-pull nature of **2** induces excited state intramolecular charge transfer (ICT), leading to solvatochromic FL and CPL, which was investigated by steady-state and time-resolved spectroscopy and quantum chemical calculations.

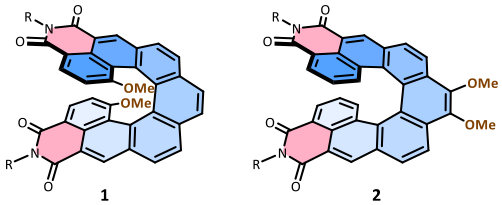


**1** Methoxy @ inner helix Through-space conjugation

**2** Methoxy @ outer helix Excited state charge transfer

**Fig. 1**. Methoxy functionalised [7]helicene diimides.

The synthesis of the target molecule **2** was achieved in three steps from **3** (Scheme 1). Employing the Bouveault aldehyde synthesis, **4** was obtained in 55% yield, which was then subjected to a piperidine-catalysed Knoevenagel condensation with *N*-(*n*-butyl)homophthalimide to yield the stilbene-type compound **5** as an isomeric mixture (*E*,*E* / *E*,*Z* / *Z*,*Z*). The subsequent oxidative photocyclodehydrogenation[24] gave a racemic mixture of compound **2.** The structure of **2** was confirmed by 2D $^{1}$H and $^{13}$C NMR spectroscopy as well as HRMS. *Rac*-**2** could be resolved into its enantiomers by HPLC on chiral stationary phase columns (Fig. S7, ESI). To evaluate the configurational stability, the Gibbs activation energy for the enantiomerization was determined to be 42.1 kcal mol$^{-1}$ (Fig. S8, ESI), which is comparable to that of [9]helicene (43.1 kcal mol$^{-1}$).[25, 26]

[a] *Julius-Maximilians-Universität Würzburg, Institut für Organische Chemie, Am Hubland, D-97074 Würzburg, Germany.*

Electronic supplementary information (ESI) available: Synthetic procedures and characterisation data for all new compounds, DFT calculations, additional optical spectroscopy data, Lippert-Mataga plot calculation, CSP-HPLC separation data, NMR and HRMS spectra, and Cartesian coordinates. See DOI: 10.1039/x0xx00000x

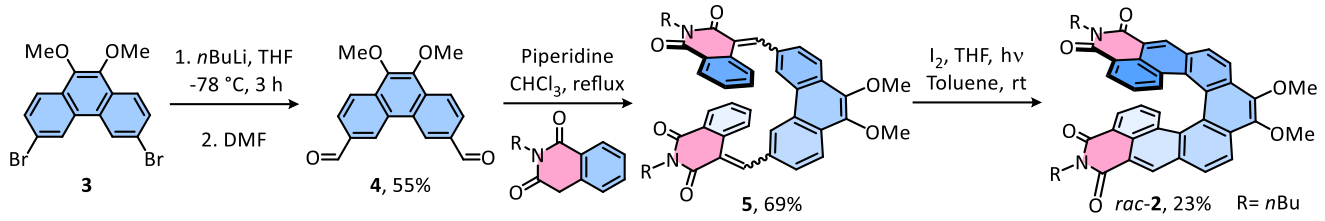


**Scheme 1**. Synthesis of *rac*-**2**.

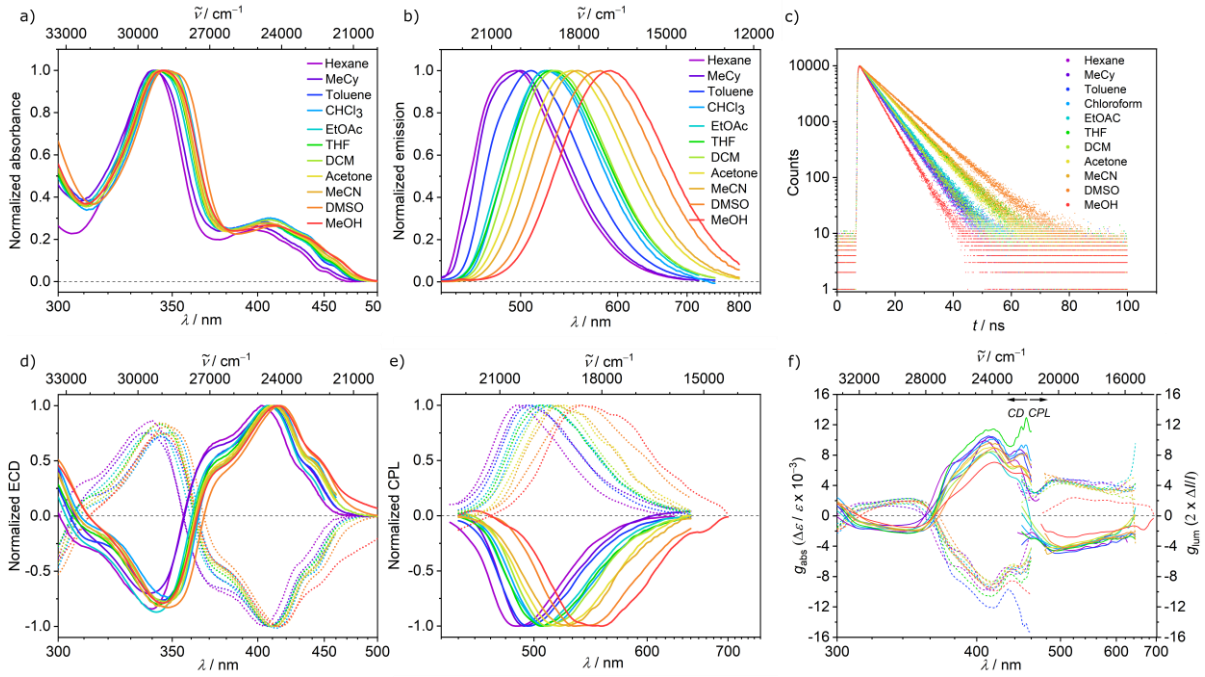


**Fig. 2.** Optical properties of **2** in solvents of various polarity. (a) UV–vis absorption ($c$ ~$10^{-5}$ M) and (b) emission ($c$ ~$10^{-6}$ M) spectra. (c) Time-resolved FL decay (excitation at 419 nm, $c$ ~$10^{-5}$ M). (d) CD and (e) CPL spectra ($c$ ~$10^{-5}$ M, *er* >99%). Solvent colour code for CD and CPL corresponds to the same for absorption and emission spectra, respectively. The solid and dotted lines correspond to the *P* and *M* isomers, respectively. (f) $g_{abs}$ and $g_{lum}$ plot.

Already during the workup and purification of **2**, a discernible redshift in FL was apparent when dissolved in higher-polarity solvents, while the inherent yellow colour of the solutions remained unchanged. A thorough spectroscopic analysis of **2** within solvents spanning a wide range of polarity (Fig. 2) validated this observation. The FL maximum of **2** exhibited a nearly linear shift from blue (495 nm) to orange (591 nm) with escalating solvent polarity resulting in an impressive apparent Stokes shift of up to 7470 $cm^{-1}$ (181 nm) in methanol (Table 1). Simultaneously, the lowest-energy absorption peak experienced only a minor displacement from 397 nm to 410 nm. The pronounced solvatochromic effects in **2** allowed us to estimate the dipole moment difference ($\Delta\mu_{eg}$) between the ground and CT excited state by a Lippert-Mataga-plot[27] (Fig. S6, ESI). The calculation yields a significant change in dipole moment $\Delta\mu_{eg}$ of 11.7 D, supporting the excited state CT character of the molecule.

FL quantum yields (FQYs) of **2** range from 0.11 in *n*-hexane up to 0.34 in DMSO, exhibiting an unusual increase in higher polarity aprotic solvents (Table 1). Along with the growth in FQYs, there is a corresponding increase in FL lifetime from 5.89 ns in *n*-hexane to 9.31 ns in DMSO (Fig. 2c). To achieve this result, the nonradiative decay rate constant ($k_{NR}$) must decrease significantly in more polar solvents from $15.6\times10^7$ $s^{-1}$ in *n*-hexane to $7.09\times10^7$ $s^{-1}$ in DMSO (Table 1). Usually, the FQY and lifetime of CT compounds decrease with increased polarity as the decreased emission energy will lead to enhanced $k_{NR}$ following the energy gap law.[28, 29] Here, the decrease of $k_{NR}$ contradicts these common observations and the Engelman-Jortner gap rule,[30] most likely because the degree of CT character decreases in less polar solvents.[31] Moreover, the nonradiative reverse-CT process in **2** is likely impeded by structure change and solvent reorganization energy, which may also contribute to the reverse energy-gap dependence of $k_{NR}$. Notably, compound **1** does not show pronounced solvatochromic effects (ESI Fig. S3) and in comparison, compound **2** exhibits enhancement in both FQY and lifetimes.

To gain insight into the photoinduced dynamics of **2** beyond that given by the time resolved fluorescence spectroscopy, we measured transient absorption (TA) spectra with fs time resolution by pumping solutions of **2** in medium polar DCM and in very polar MeCN and probed the transient states by time-delayed white light between 400–800 nm with an IRF of 100 fs. The transient spectra were corrected for stray light and chirp

and globally deconvoluted using GLOTARAN software[32] applying a sequential model of states with exponential kinetics yielding evolution associated difference spectra (EADS) with increasing order of lifetimes (Fig. 3). In both solvents, two EADS with lifetimes of 1.1 and 12 ps in DCM and of 0.6 ps and 5.5 ps in MeCN indicate a slow process that leads to the formation of the $S_1$ state. Hereby, the first EADS with lifetime ≈ 1 ps is typical of solvent relaxation[33] upon CT and the longer component is most likely caused by internal vibrational relaxation of the $S_1$ state.[34] This process is completed within a few ps and yields the third EADS which refers to the relaxed $S_1$ state with CT character. This EADS shows a prominent peak at 490 nm but also a distinct shoulder at ca. 540 nm and a lifetime of 7.7 ns in DCM and 7.4 ns in MeCN, both in good agreement with the fluorescence lifetime. A fourth EADS with a distinct broad peak at ca. 600 nm and with lifetimes in both solvents beyond that measurable with our set-up indicates the formation of a triplet state.

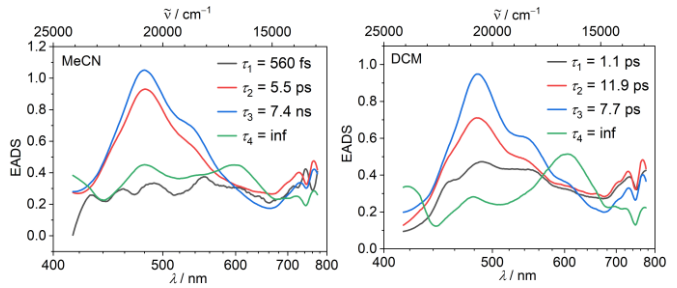


**Fig 3.** Evolution associated difference spectra (EADS) of a global deconvolution of fs-TA spectra in MeCN and DCM (excitation at 407 and 408 nm, respectively).

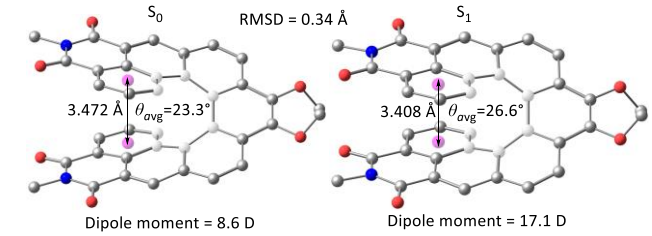


**Fig 4.** Ground ($S_0$) and excited ($S_1$) state optimised geometries of **2** in the gas phase and acetonitrile, respectively. Hydrogen atoms are omitted for clarity.

DFT calculations (at the ωB97XD/6-31g(d,p) level) provided further insights into the excitation-emission process and geometries of the ground and excited $S_1$ states (Section S8, ESI). Considerable disparities are observed between the $S_0$ and $S_1$ states geometries with a root mean square displacement (RMSD) of 0.34 Å (Fig. 4). The substantial structural reorganization occurring during the excitation-emission process provides a rational explanation for the broad emission with pronounced Stokes shifts, even in non-polar solvents.[35] Furthermore, to assess the influence of the solvent, optimization of the $S_1$ state geometry was carried out accounting for solvent effects. Interestingly, the incorporation of the solvent exhibited a minimal alteration in the molecular geometry but a consistent increase in dipole moment with more polar solvents, confirming the dependence of CT character on solvent polarity (Fig. S10, ESI). Consequently, the noteworthy augmentation of the Stokes shift in polar solvents can be ascribed to their propensity to stabilize the CT excited state. Moreover, TD-DFT calculations revealed that the lowest energy excitation is mainly stemming from the HOMO→LUMO transition with an oscillator strength of 0.08.

To investigate the chiroptical properties of **2,** CD and CPL measurements were performed in solvents of varying polarity. The absolute configuration of **2** was assigned by comparing the experimental CD spectra with the one calculated by TD-DFT (Fig. S11, ESI). Following the trend of UV–vis, the CD spectra look similar in all solvents, showing a pronounced peak at the first maximum before changing sign at shorter wavelengths. The absorption dissymmetry factor ($g_{abs}$) shows a maximum at the lowest-energy absorption maximum, with a magnitude of ~$10^{-2}$ in all investigated solvents (Table 1). The CPL spectra show a similar shape to the FL spectra, albeit with a somewhat smaller bathochromic shift in higher-polarity solvents. This observation can be explained by the fact that the maxima of the luminescence dissymmetry factor ($g_{lum}$) values lie towards the higher-energy edge of the emission spectra, with values on the order of ~$0.45\times10^{-2}$ in aprotic solvents (Table 1). The similar $g_{abs}/g_{lum}$ ratio of ~0.5 in all aprotic solvents indicates large structural relaxation and similar excited state geometry in all solvents in corroboration with DFT optimised geometry of the $S_0$ and $S_1$ states (Fig. 4).[36] The considerably improved $g_{abs}$ for the $S_1 \leftarrow S_0$ transition and $g_{lum}$ values of **2** compared to **1** can be attributed to the decreased angle between the electric ($\mu_e$) and magnetic ($\mu_m$) transition dipole moments (Table S3, ESI).[37]

The electrochemical behaviour of **2** was examined using cyclic voltammetry (CV). The CV analyses in THF unveiled one reversible two-electron reduction wave (Fig. S5, ESI) at 1.73 V vs the $Fc/Fc^+$ redox couple. This contrasts with **1**, where two discernible reduction couples are separated by 0.23 V. Notably, the absence of a second reduction wave in **2** indicates minimal electronic interactions between the two imide units. This is further supported by the calculated IV-CT parameters[38] (Table S4, ESI) and weaker electronic coupling ($V_{12}$) value (727 $cm^{-1}$) for **2** than for **1** (1362 $cm^{-1}$). An analysis of the frontier molecular orbitals of **1** and **2** highlights the similarities between the LUMOs but a stark difference in the HOMOs (Fig. S9, ESI). The methoxy group of **1** largely localizes the HOMO at the inner helix providing significant through-space orbital overlap. Therefore, the reduced electronic coupling between the imide moieties in **2** can be attributed to weakened through-space interactions at the inner helix.

In summary, we have shown a straightforward synthesis of the helically chiral push-pull molecule **2**. In comparison to **1**, strategic repositioning of the methoxy groups to the outer helix leads to distinct photophysical and electrochemical properties. Our investigations shed light on the complex interplay between ICT, molecular geometry, and chiroptical properties in **2**. In particular, a much higher dipole moment in the excited state leads to pronounced fluorosolvatochromism with the emission maximum spanning almost the entire visible spectrum and a halved $g_{lum}$ value (~$0.5\times10^{-2}$) compared to the $g_{abs}$ factor of up to ~$1\times10^{-2}$. Compound **2** exhibits unique features such as

enhanced FQY and lifetimes with increase in solvent polarity, reverse energy-gap dependence of $k_{NR}$, and consistent $g_{abs}$ and $g_{lum}$ values in aprotic solvents. The improved chiroptical properties compared with the previously synthesised compound **1** highlight the potential of the helicene diimide class of molecules to tune the compounds' properties by varying the functional groups. The sterically exposed methoxy groups of **2** also provide an avenue for derivatization of the compound to further investigate the influence of functional groups on the properties of HDIs.

**Table 1.** Summary of optical properties of **2** in selected solvents.

| Solvent | $f(D)–f(n^2)$[a] | $\lambda_{abs}$ /nm | $\lambda_{em}$ / nm | $\Delta\nu$ / $cm^{-1}$ | $\tau_{FL}$ / ns | $E_g$[b]/ eV | $\Phi_{FL}$ | [c]$k_{FL}$ / $10^7$ $s^{-1}$ | [d]$k_{NR}$ / $10^7$ $s^{-1}$ | *FWHM*[e] / $cm^{-1}$ | $g_{abs}$ /$10^{-3}$ | $g_{lum}$/ $10^{-3}$ |
|---|---|---|---|---|---|---|---|---|---|---|---|---|
| Hexane | 0.00 | 397 | 495 | 4987 | 5.71[b] | 2.78 | 0.11 | 1.93[c] | 15.6[c] | 3221 | 9.8 | 4.5 |
| Toluene | 0.01 | 405 | 509 | 5045 | 5.97 | 2.72 | 0.18 | 3.01 | 13.7 | 3626 | 11.2 | 5.0 |
| DCM | 0.22 | 408 | 532 | 5713 | 6.01 | 2.66 | 0.26 | 4.33 | 12.3 | 3755 | 8.6 | 4.2 |
| MeCN | 0.31 | 408 | 554 | 6459 | 8.05 | 2.63 | 0.25 | 3.11 | 9.32 | 3979 | 9.5 | 4.4 |
| DMSO | 0.26 | 414 | 579 | 6883 | 9.31 | 2.60 | 0.34 | 3.65 | 7.09 | 4185 | 8.9 | 4.2 |

[a]Lippert-Mataga solvent polarity function. [b] Optical energy gap estimated from the crossing of absorption and FL spectra. [c]Rate constant for the radiative decay $k_{FL}= \Phi_{FL}/\tau_{FL}$. [d]Rate constant for the non-radiative decay $k_{NR} = (1-\Phi_{FL})/\tau_{FL}$. ESI Table S1 includes all the solvents. [e]Full width at half maximum of FL spectra.

## Conflicts of interest

"There are no conflicts to declare".

## Notes and references

We thank European Research Council (ERC) (ERC-Starting Grant, Project no. 101041464) for financial support. The CPL/CD hybrid spectrometer was funded by the DFG (Project No. 444286426).

1. P. Osswald and F. Würthner, *J. Am. Chem. Soc.*, 2007, **129**, 14319.
2. C. Lütke Eversloh, Z. Liu, B. Müller, M. Stangl, C. Li and K. Müllen, *Org. Lett.*, 2011, **13**, 5528.
3. H. Bock, D. Subervie, P. Mathey, A. Pradhan, P. Sarkar, P. Dechambenoit, E. A. Hillard and F. Durola, *Org. Lett.*, 2014, **16**, 1546.
4. N. Liang, D. Meng and Z. Wang, *Acc. Chem. Res.*, 2021, **54**, 961.
5. F. Saal and P. Ravat, *Synlett*, 2021, **32**, 1879.
6. J. Li, P. Li, M. Fan, X. Zheng, J. Guan and M. Yin, *Angew. Chem. Int. Ed.*, 2022, **61**, e202202532.
7. W. Jiang and Z. Wang, *J. Am. Chem. Soc.*, 2022, **144**, 14976.
8. S. T. Bao, H. Jiang, Z. Jin and C. Nuckolls, *Chirality*, 2023, DOI: https://doi.org/10.1002/chir.23561.
9. T. Kogiso, K. Yamamoto, H. Suemune and K. Usui, *Org. Biomol. Chem.*, 2012, **10**, 2934.
10. N. J. Schuster, D. W. Paley, S. Jockusch, F. Ng, M. L. Steigerwald and C. Nuckolls, *Angew. Chem. Int. Ed.*, 2016, **55**, 13519.
11. B. Liu, M. Böckmann, W. Jiang, N. L. Doltsinis and Z. Wang, *J. Am. Chem. Soc.*, 2020, **142**, 7092.
12. C. Weiss, D. I. Sharapa and A. Hirsch, *Chem. Eur. J.*, 2020, **26**, 14100.
13. L. Zhang, I. Song, J. Ahn, M. Han, M. Linares, M. Surin, H.-J. Zhang, J. H. Oh and J. Lin, *Nat. Commun.*, 2021, **12**, 142.
14. J. Tan, G. Zhang, C. Ge, J. Liu, L. Zhou, C. Liu, X. Gao, A. Narita, Y. Zou and Y. Hu, *Org. Lett.*, 2022, **24**, 2414.
15. V. B. R. Pedersen, S. K. Pedersen, Z. Jin, N. Kofod, B. W. Laursen, G. V. Baryshnikov, C. Nuckolls and M. Pittelkow, *Angew. Chem. Int. Ed.*, 2022, **61**, e202212293.
16. X. Tian, K. Shoyama, B. Mahlmeister, F. Brust, M. Stolte and F. Würthner, *J. Am. Chem. Soc.*, 2023, **145**, 9886.
17. F. Saal, F. Zhang, M. Holzapfel, M. Stolte, E. Michail, M. Moos, A. Schmiedel, A.-M. Krause, C. Lambert, F. Würthner and P. Ravat, *J. Am. Chem. Soc.*, 2020, **142**, 21298.
18. J. B. Birks, D. J. S. Birch, E. Cordemans and E. Vander Donckt, *Chem. Phys. Lett.*, 1976, **43**, 33.
19. Y. Nakai, T. Mori and Y. Inoue, *J. Phys. Chem. A*, 2012, **116**, 7372.
20. M. Li, H.-Y. Lu, C. Zhang, L. Shi, Z. Tang and C.-F. Chen, *Chem. Commun.*, 2016, **52**, 9921.
21. H. Sakai, T. Kubota, J. Yuasa, Y. Araki, T. Sakanoue, T. Takenobu, T. Wada, T. Kawai and T. Hasobe, *J. Phys. Chem. C*, 2016, **120**, 7860.
22. K. Dhbaibi, L. Favereau, M. Srebro-Hooper, C. Quinton, N. Vanthuyne, L. Arrico, T. Roisnel, B. Jamoussi, C. Poriel, C. Cabanetos, J. Autschbach and J. Crassous, *Chem. Sci.*, 2020, **11**, 567.
23. F. Bureš, *RSC Adv.*, 2014, **4**, 58826.
24. F. B. Mallory and C. W. Mallory, in *Organic Reactions*, John Wiley & Sons, Inc., 2005, DOI: 10.1002/0471264180.or030.01, pp. 1.
25. R. H. Martin and M. J. Marchant, *Tetrahedron*, 1974, **30**, 347.
26. P. Ravat, *Chem. Eur. J.*, 2021, **27**, 3957.
27. N. Mataga, Y. Kaifu and M. Koizumi, *Bull. Chem. Soc. Jpn.*, 1955, **28**, 690.
28. R. Stahl, C. Lambert, C. Kaiser, R. Wortmann and R. Jakober, *Chem. Eur. J.*, 2006, **12**, 2358.
29. A. Ito, K. Kawanishi, E. Sakuda and N. Kitamura, *Chem. Eur. J.*, 2014, **20**, 3940.
30. R. Englman and J. Jortner, *Mol. Phys.*, 1970, **18**, 145.
31. I. R. Gould and S. Farid, *J. Phys. Chem. B*, 2007, **111**, 6782.
32. J. J. Snellenburg, S. Laptenok, R. Seger, K. M. Mullen and I. H. M. van Stokkum, *Journal of Statistical Software*, 2012, **49**, 1
33. M. L. Horng, J. A. Gardecki, A. Papazyan and M. Maroncelli, *J. Phys. Chem.* , 1995, **99**, 17311.
34. T. Kumpulainen, B. Lang, A. Rosspeintner and E. Vauthey, *Chem. Rev.*, 2017, **117**, 10826.
35. Z. R. Grabowski, K. Rotkiewicz and W. Rettig, *Chem. Rev.*, 2003, **103**, 3899.
36. H. Tanaka, Y. Inoue and T. Mori, *ChemPhotoChem*, 2018, **2**, 386.
37. H. Kubo, T. Hirose, T. Nakashima, T. Kawai, J.-y. Hasegawa and K. Matsuda, *J. Phys. Chem. Lett.*, 2021, **12**, 686.
38. J. Schäfer, M. Holzapfel, B. Mladenova, D. Kattnig, I. Krummenacher, H. Braunschweig, G. Grampp and C. Lambert, *J. Am. Chem. Soc.*, 2017, **139**, 6200.